IMPACT: A facility to study the interaction of low-energy intense particle beams with dynamic heterogeneous surfaces

J. P. Allain,[a] M. Nieto, M. R. Hendricks, P. Plotkin, S. S. Harilal, and A. Hassanein
Argonne National Laboratory, 9700 S. Cass Avenue, Argonne, Illinois 60439, USA

(Received 19 April 2007; accepted 14 October 2007; published online 14 November 2007)

The Interaction of Materials with Particles and Components Testing (IMPACT) experimental facility is furnished with multiple ion sources and *in situ* diagnostics to study the modification of surfaces undergoing physical, chemical, and electronic changes during exposure to energetic particle beams. Ion beams with energies in the range between 20 and 5000 eV can bombard samples at flux levels in the range of 10^{10}–10^{15} cm^{-2} s^{-1}; parameters such as ion angle of incidence and exposed area are also controllable during the experiment. IMPACT has diagnostics that allow full characterization of the beam, including a Faraday cup, a beam imaging system, and a retarding field energy analyzer. IMPACT is equipped with multiple diagnostics, such as electron (Auger, photoelectron) and ion scattering spectroscopies that allow different probing depths of the sample to monitor compositional changes in multicomponent and/or layered targets. A unique real-time erosion diagnostic based on a dual quartz crystal microbalance measures deposition from an eroding surface with rates smaller than 0.01 nm/s, which can be converted to a sputter yield measurement. The monitoring crystal can be rotated and placed in the target position so that the deposited material on the quartz crystal oscillator surface can be characterized without transfer outside of the vacuum chamber.
 [DOI: 10.1063/1.2805677]

I. INTRODUCTION

The study of surfaces and interfaces and their interaction with energetic particles during thin film growth and nanostructure fabrication has inspired the design of advanced *in situ* characterization experiments and experimental facilities.[1–5] In addition, designing experiments that simulate complex environments (e.g., particle irradiation of multicomponent surfaces) and the ability to diagnose individual mechanisms and properties have become vital for computational modeling benchmarking.[6–8] Computational codes have become vital in complementing and extending understanding of the fundamental processes during synthesis of nanoscale structures and ultrathin film systems.

Tailoring functional and dynamic properties of future nanoscale devices and systems requires knowledge of how these properties behave both on broad temporal and spatial scales. Heterogeneous thin film growth and synthesis of advanced materials using energetic particle bombardment also require insight of the elemental, chemical, and structural state evolutions during particle irradiation. The low-dimensional states inherent in nanostructure systems at a surface (i.e., metal clusters, nanostructure island coalescence, interface modification) demand a set of complementary surface-sensitive characterization tools able to resolve a complex set of variables in space and time. For example, hyperthermal (500–1000 eV) Sn ions are an ultrashallow implant in Ru thin film mirrors penetrating a few monolayers (1–2 nm) below the air/film interface. The implanted species affect the optical reflective properties of the mirror at wavelengths that approach the implantation zone. This particular phenomenon is important in 13.5 nm extreme ultraviolet lithography used for future nanometer scale feature sizes.[9–13]

In another application, surfaces and interfaces of thin films used in the fabrication of advanced nonvolatile memories require the use of sophisticated characterization systems to adequately diagnose the chemical, kinetic, and thermodynamic behaviors of the thin films and the material integration strategies required for the development of next-generation devices. This is particularly important when characterizing ultrathin interfacial zones relevant to the compatibility and performance of ultrathin dielectric materials for next-generation complementary metal-oxide-semiconductor devices.[1]

The Interaction of Materials with Particles and Components Testing (IMPACT) experimental facility has been designed to study *in situ* dynamic heterogeneous surfaces at the nanoscale exposed to varied environments that modify surface and interface properties. The philosophy behind experiments in IMPACT relies heavily on its ability to provide a wide array of characterization techniques and conditions that properly simulate complex environments. The IMPACT experiment achieves this by atomic-scale characterization of the evolution of elemental, chemical, and thermodynamic states of ultrathin film surface and interfaces using complementary surface-sensitive characterization techniques. *In situ* techniques used in the IMPACT experiment include low-energy ion scattering spectroscopy (LEISS) with simultaneous forward and backward scattering modes, direct recoil spectroscopy (DRS) (to study impurity levels in the film), x-ray photoelectron spectroscopy (XPS), Auger electron

[a]Author to whom correspondence should be addressed. Electronic mail: allain@purdue.edu

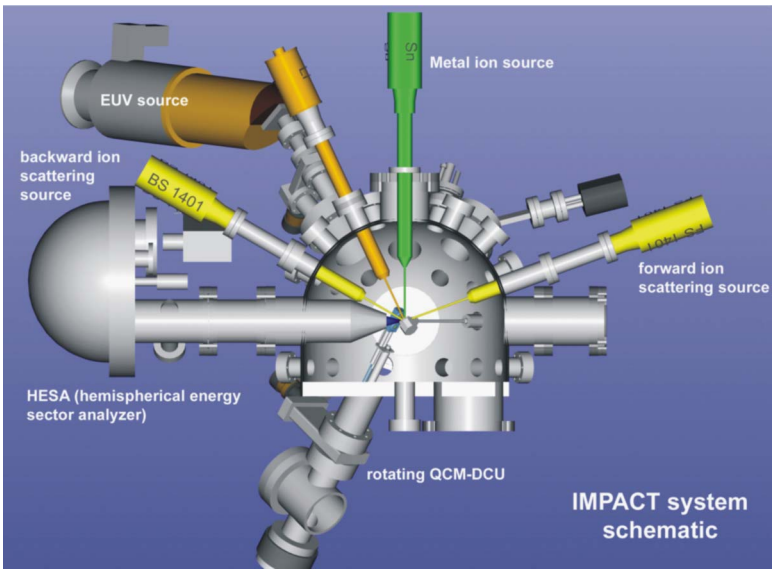

FIG. 1. (Color online) Schematic of the IMPACT experimental facility with selected excitation sources and *in situ* diagnostic systems. The facility is equipped with several ions sources, x-ray (not shown) and EUV sources, hemispherical energy analyzer (HSA), mass spectrometers (not shown), QCM-DCU, etc.

spectroscopy (AES), extreme ultraviolet (EUV) (13.5 nm) reflectometry (EUVR), extreme ultraviolet photoelectron spectroscopy (EUPS), and mass spectrometry using both quadrupole and magnetic sector analyzers. EUPS combined with LEISS can give chemical state and elemental information at the first two to three monolayers (MLs), respectively. AES and XPS give similar information at probing depths from two to three monolayers down to about 10–15 nm into the bulk of a thin film.

Both ion and electron spectroscopies are conducted using a highly sensitive hemispherical energy multichannel analyzer. High-resolution depth profiles are obtained by using a unique low-energy ion source delivering 100 eV ions of any desired inert gas species at current densities of 2.5 $\mu A/cm^2$. Simultaneous to surface analysis of the irradiated sample, the total erosion flux is measured *in situ* using an ultrasensitive temperature-compensating quartz crystal nanobalance dual crystal unit with resolution better than 0.005 Å/s. During ion etching the sample can be tilted at any desired angle with respect to its surface normal from 0° to 60° with a resolution of better than 0.1°. Dynamic effects induced by energetic charged particles can range from induced surface morphology evolution to physical sputtering. IMPACT is designed to primarily study the effects of the latter by means of mass loss techniques.

This paper is organized in the following manner. The first section describes auxiliary systems for the IMPACT experiment. This is followed by a description of the various ion sources and ion beam diagnostics. Then a description of IMPACT photon sources is followed by a description of the evaporation system and its calibration. The IMPACT experimental setup is concluded by a description of the hemispherical energy sector analyzer and quartz crystal microbalance dual crystal unit (QCM-DCU). The paper then presents details of surface analytical techniques used in IMPACT. Results and discussion for a "model" experiment is described followed by a short summary.

II. IMPACT EXPERIMENT

A. Chamber and target delivery

The basic experimental setup is first made up of key auxiliary systems. Auxiliary systems in IMPACT consist of three major components: the vacuum system, the sample transfer system, and the gas delivery system. One of the most vital components of the IMPACT experimental facility is the design of the vacuum chamber, custom-made to provide functionality and versatility. Figure 1 shows the schematic of the main vacuum chamber with various radiation/particle sources and diagnostic tools. The IMPACT vacuum chamber is equipped with 55 ports and each port is designated for a particular application.

The vacuum system in IMPACT consists of two oil-less scroll pumps, a turbomolecular pump, and an ion pump. Ion sources and supplementary chambers (i.e., load locks, transfer chambers, preparatory chambers) are differentially pumped. The pressure achieved with just the roughing pump is around 0.1 Pa, and the rate of rise in the chamber is typically less than 0.05 Pa/min. Once the ultimate pressure of the rough pump is reached, the gate valve to an oil-less Leybold magnetically levitated turbomolecular pump is opened, and the chamber is taken to a pressure of less than 1×10^{-4} Pa in a few hours. If the vacuum chamber has been vented for an extended period of time or exposed to a humid environment, an internal halogen lamp is used to help eliminate adsorbed water on internal chamber surfaces. Once the pressure is less than 1×10^{-4} Pa, a gate valve is opened to the ion pump. The GV TiTan ion pump is a 350 l/s system equipped with Ti sublimation elements that increase the pumping efficiency. With the ion pump open, IMPACT reaches the ultimate pressure, around 1×10^{-7} Pa. IMPACT facility is also equipped with two mass spectrometers (quadrupole and magnetic sector analyzers). The partial pressures of the background gases in the chamber during the experiments are monitored with these mass spectrometer systems. When measuring chemical sputter yields, the data from these

analyzers are corrected for species fragmentation and contributions from sources outside the sample.[14]

The sample transfer system in IMPACT allows higher sample throughput, since venting of the system is avoided. Samples are placed in sample platens especially constructed to fit on the platen holder inside of IMPACT. The platen is placed in a small chamber with a quick-vent style door, sitting on top of a fork-shaped holder mounted at the end of a long (2 m) magnetically coupled linear travel arm. Once the sample is in the fork holder, the small chamber is evacuated using a turbopump. Once the pressure in the load-lock chamber is less than 1×10^{-4} Pa, an opening between the load-lock and the IMPACT chamber is opened using a gate valve, and the fork holder is inserted. Since the travel arm is mounted on a pivoting base, the travel arm can be flexed up and down with high precision by using a screw and a custom-engineered hinge. Once the platen with the sample is placed in the platen holder inside IMPACT, the travel arm is retracted and the opening between the load-lock and the IMPACT chamber is closed. To extract a sample, the process is repeated in reverse. Up to three to four samples can also be stored inside the main chamber for cases of multiple-sample analysis. The gas delivery system in IMPACT injects high-purity gases (>99.999% purity) to the differentially pumped ion sources via a manually controlled valve.

B. Ion sources

The charged-particle beam sources in IMPACT play a key role in the experiment both as excitation/probing sources (i.e., secondary electron emission, ion scattering spectroscopy) and as modifying sources (i.e., implantation, ion-induced desorption, etching, etc.). They also provide a means to simulate conditions found in prototype devices such as plasma processing devices or fusion reactor systems. Currently IMPACT has four specialized sources, each one with a specific function and a unique capability. All the ion sources currently installed are hot filament sources, except for one based on thermionic emission. The following subsections describe each ion source with both its capability and application.

1. High-energy ion source

A high-energy ion source (NTI 1401) (Ref. 15) installed in IMPACT is capable of operating with all noble gases and a few reactive gases including hydrogen, nitrogen, and oxygen. The ion source consists of an electron impact ionization source. Electrons are emitted from the energized filament and are accelerated through an electrode screen surrounding the source region making ionization collisions with atoms of the source gas. The ions thus produced are extracted and accelerated to their final energy and then pass into the condenser lens. Its multiple optical elements allow full control over the beam spot size, as well as a long working distance, so that submillimeter beam spots can be obtained 10 cm away from the source exit. The incident ion current on surfaces can be varied by changing the electron emission current. An octopole ion optics element at the ion-gun shaft exit provides rastering capabilities that result in flexibility on the size of area exposed to the beam and consequently a secondary control of the ion flux. Ion fluxes in the range between 10^{10} and 10^{15} cm^{-2} s^{-1} are routinely achieved. The ion energy range for this source is between 100 eV and 5 keV, although lower energies are possible at the cost of both current and beam size. The dependence of the NTI 1401 ion source flux against ion energy is plotted in Fig. 2 and is compared to another ion source summarized below. The NTI 1401 ion source is mostly used as a diagnostic tool for LEISS. The ion source is also utilized for sample cleaning when other methods are not sufficient or available.

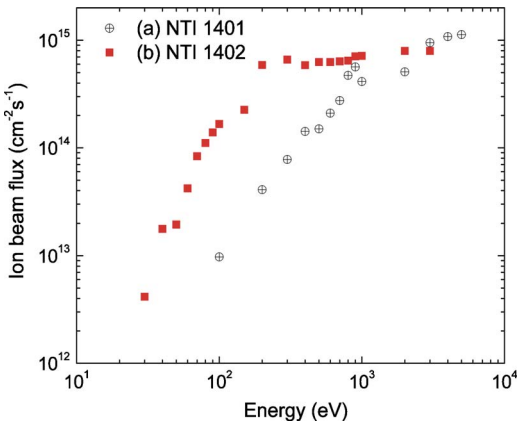

FIG. 2. (Color online) Plot of ion beam flux vs energy for two ion sources in IMPACT (a) high-energy ion source NTI 1401 and (b) low-energy ion source NTI 1402. For estimating ion flux at the target surface, spot size measurements were made using five-pinhole Faraday cup method.

2. Low-energy ion source

A low energy ion source (NTI 1402) (Ref. 16) installed in IMPACT is similar in design to the NTI 1401 but with modified optics to allow ion extraction at lower energies, even below 100 eV. The spot size and current can be controlled by the user, but due to the nature of the extraction process, the maximum flux is reduced to about 10^{14} cm^{-2} s^{-1} for the case of ion beams with energies below about 80–90 eV, as shown in Fig. 2. To assess the energy spread of the low-energy ion source, we measured it with a retarding field analyzer (RFA) (details of RFA are given in Sec. II B 5) and the data for three energies (50, 100, and 150 eV) of a singly charged Ar^+ beam are shown in Fig. 3. The plot shows

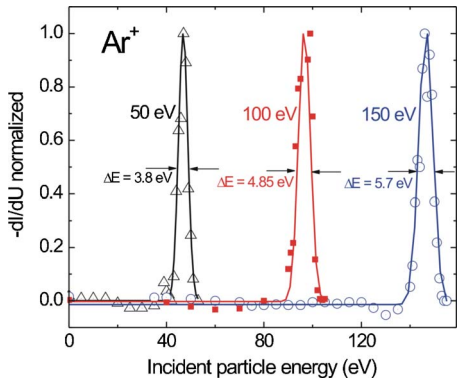

FIG. 3. (Color online) Energy spread of 50, 100, and 150 eV Ar^+ beams measured with a retarding field analyzer. The plot shows the negative derivative of the normalized current with respect to applied voltage.

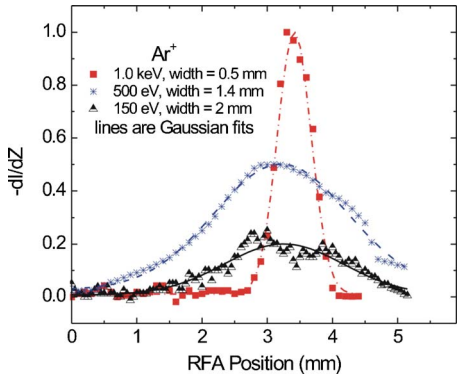

FIG. 4. (Color online) Spatial profiles of singly charged argon ion beams at different impact energies. The ion source used NTI 1402 and the measurement is conducted by moving the retarding field analyzer with a step width of 0.05 mm.

the negative derivative of the normalized current versus applied voltage data for each of the incident energies. The energy spread is 3.8%, 4.9%, and 5.7% for 50, 100, and 150 eV, respectively, with a Gaussian centroid shift no more than 3.0 eV from the applied voltage of the ion source. As the ion beam energy decreases, the size of the beam starts to increase due to Coulomb repulsion, as shown in Fig. 4, which shows the spatial profile of ion beams with different impact energies. The measurement is conducted by moving the RFA manipulator arm linearly with a resolution of 0.05 mm.

3. Metal ion source

IMPACT consists of a metal ion source (NTI 14MS) (Ref. 17) currently operated with Sn but upgradable to metals with relatively low vapor pressures. The metal ion source utilizes electron impact ionization of a pure metal vapor derived by an internal heater. The gun is also designed to operate with inert gaseous species and with some reactive gases. In addition to an optical column similar to the other ion sources, the 14MS is also equipped with a Wien filter with a 3° bend, which filters particles with a particular mass to charge ratio to exit the gun. The separation is done by varying the current on the filter's electromagnet, enabling the selection of the mass or charge state of the ion. When the 14MS source is operated with metal ions, its primary function is that of implantation and near-surface modification. Typical operational energies used with Sn ions range from 500 to 2000 eV, depending on the particular experiment. An example of its use on exposure of metal thin films is given in Sec. IV.

4. Lithium ion source

Another source installed in IMPACT is a Li ion source. Unlike all the previous ones, this source does not operate with gas, only with its internal Li charge. This is because the main principle for ion generation is via the thermionic process. A lithium impregnated ceramic surface is heated to very high temperatures, thus emitting Li atoms in the ionic charge state. Fluxes up to 10^{14} cm^{-2} s^{-1} in the energy range between 500 and 5000 eV can be achieved with this source. The Li alkali-metal source is used for two applications in IMPACT. One is the use as an implanting species during simulated experiments of tokamak plasma-facing surfaces. Recent studies have focused on the use of lithium as a plasma-facing component in tokamak plasmas and thus interest exists for measurement of fusion candidate materials under Li ion bombardment simulating redeposition of sputtered Li particles.[18] The second application has not been pursued substantially and it consists of using Li ions for low-energy ion scattering for structural analysis of metal surfaces. This is possible due to the relatively high probability of ionization of Li atoms scattering from metal surfaces. Thus, unlike inert gas scattered particles, Li ions scattered from surfaces can give information from subsurface atoms (below two to three MLs), thus yielding structure details.[19]

5. Ion beam diagnostics

Since ion beams are critical for performing studies in the IMPACT facility, it is imperative to count with adequate diagnostics that measure ion beam parameters such as size, intensity, and energy. A variety of diagnostics are used in the characterization of ion beams in IMPACT. The diagnostics consist of a partially oxidized alkali-metal screen, a five-pinhole Faraday cup, and a RFA. Each diagnostic has distinct functions and each is used for particular calibration tests prior to performing experimental runs in IMPACT.

The ion current is measured directly from the target in series with a grounded Keithley 6487 picoammeter. We conducted a test for measuring ion-induced secondary electron emission and found that the secondary electron contribution is less than 10% for energies higher than 100 eV. For avoiding secondary electron emission at lower energy levels ($<$100 eV), a positive charged bias voltage is applied to the target.

A partially oxidized lithium metal screen is used for probing the location of the ion beam on the target surface. The lithium diagnostic takes advantage of the 671 nm Li I line emission, excited when incident energetic inert gas ions collide with surface Li atoms. The emitted light is an indirect measurement of the size of the ion beam and direct measurement of its location. This diagnostic is mainly used for positioning of the beam and measuring of the general beam raster areas, allowing a rough estimate of the ion flux in combination with the ion beam current measured in series with a picoammeter. The alkali-metal screen cannot be used for beams with less than 200 eV of energy or ion beam currents less than 50 nA as the light emission is rather low to be detected by a charge coupled device camera.

A five-pinhole Faraday cup is used to measure the beam current and profile the shape of the beam. This diagnostic is actually *two* Faraday cups, one nested beneath the other. The floor of the upper cup is a thin metal plate containing five 125 μm pinholes, evenly spaced 1.5 mm apart in a cross pattern. The upper Faraday cup captures the entire beam flux and is used to measure the *total* beam current. When the upper cup is grounded and one measures the output of the lower cup, a partial current is measured due to the fraction of beam flux that passes through a single hole in the pinhole plate. Using a software to control the octopole deflection lenses at the aperture of the ion-gun column, the beam is

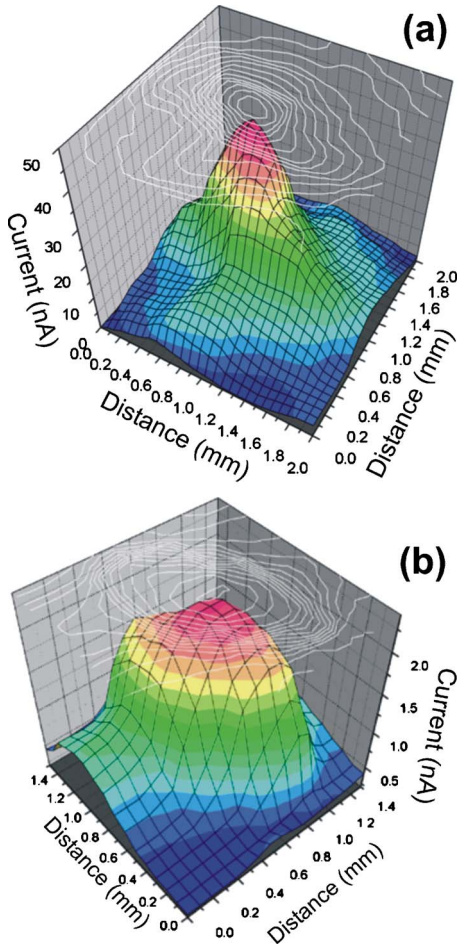

FIG. 5. (Color online) Ion profiles obtained with five-pinhole Faraday cup. The ions beam profiles are representative of 1 keV Xe^+ with 2 μA. The changes in the profiles of ions beams are obtained by changing the ion optics settings. The figures clearly indicate the utility of five-pinhole Faraday cup for analyzing spatial features of ion beams.

deflected in a rectangular array of points, and a partial current is measured at each beam position. These partial currents are logged and arranged in a two-dimensional matrix that can be plotted and analyzed, as shown in Figs. 5(a) and 5(b) for cases of 1 keV Xe^+ beams. The figures clearly indicate the utility of a five-pinhole Faraday cup for analyzing spatial features of ion beams. The advantage of this instrument is generation of two-dimensional shape profiles; however, it is limited to profiling of beams smaller than 3 mm in diameter. This instrument's primary disadvantage is the time required for both acquisition and setup during calibration tests. This diagnostic is therefore performed only once for calibration purposes for a collection of experiments under similar ion-exposure conditions.

The diagnostics described above can be used to measure the size of the ion beam and its location, but this measurement gives no information about the energy distribution of the beam. Determining whether the ion source energy peaks at the value specified by the controller setting during operation is very important, in particular, for applications that rely on low-energy ion-induced surface studies. In addition, any significant energy spread can influence the spectral response during ion scattering, thus introducing uncertainty in mass

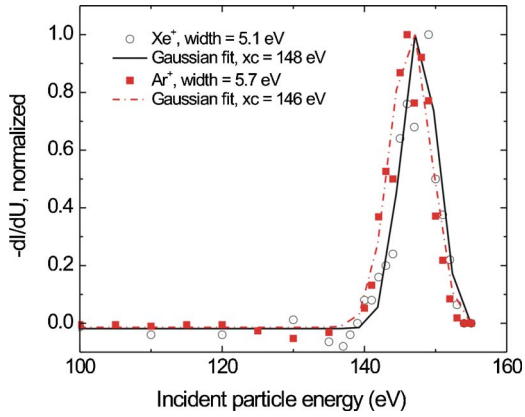

FIG. 6. (Color online) The energy spread of 150 eV Ar^+ and Xe^+ ion beams is given. The measurements are done with a retarding field analyzer. The symbols represent the experimental data points and smooth curves give the Gaussian fit. The energy spread as well as peak energy value (x_c) are also given in the figure.

identification. To perform energy distribution measurements, a RFA similar to the type used by Jacob *et al.*[2] was constructed. The RFA consists of a grounded metal tube containing three grids and a plate, all electrically isolated from its housing. A metal plate with a hole, also isolated from the body, covers the entrance to the RFA. The diameter of the entrance orifice is 6 mm and the grids are separated by 2.5 mm. The diagnostic is mounted on a linear manipulator with 0.05 mm resolution, so it can be used to profile the beam without having to raster it, as is the case for the pinhole Faraday cup. The beam is aligned such that the current read in the top plate is minimized and the current in the collector plate at the bottom of the RFA is maximized. Once this condition is met, the RFA is moved either in or out, and the current on the collector is recorded as a function of distance from the maximum current position; this allows the measurement of the beam profile in one dimension. To measure the energy distribution of the beam, the top plate and the top grid of the RFA are grounded. The bottom grid is biased with a voltage between 0 and a value 1.1 times the nominal beam energy in eV. The collector plate records the current as a function of bias voltage, and by taking the derivative of these data, the energy spread of the beam can be calculated. Figure 6 shows the measurements for 150 eV argon and xenon ion beams.

C. Photon sources

1. X-ray source

IMPACT has a dual-anode (Mg and Al), actively cooled x-ray source used to perform XPS studies. The main advantage of using a dual anode is that the presence of two different excitation energies enables rapid distinction of Auger electron lines from photoelectron structures in an XPS spectrum. The Mg and Al anodes in the x-ray source produce radiation lines at 1253.6 and 1486.6 eV. A flux of 10^{11}–10^{12} photons/s emanates from the source, which translates into a photocurrent of 40–50 nA, depending on the material. The x rays flood a circular area of about 1–2 cm^2. The footprint of the x-ray beam can be changed by modify-

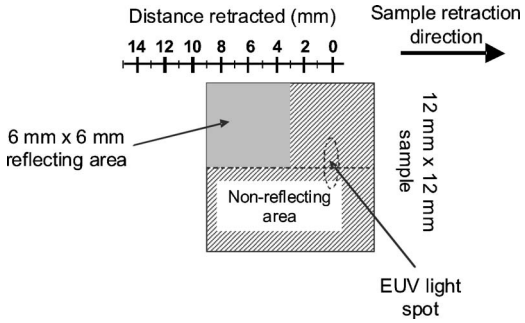

FIG. 7. Layout and scales for the EUV spot size measurement experiment. Three quadrants of the EUV reflecting surface is covered with a nonreflecting material.

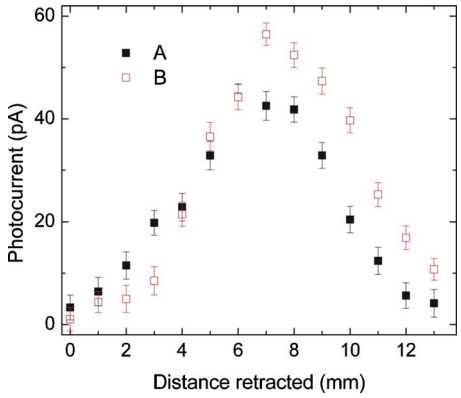

FIG. 8. (Color online) Photocurrent measured by the detector in the reflecting location. The results of the measurements are shown for the sample orientation shown in Fig. 7 (A, filled square symbols) and after rotating the sample 90° counterclockwise (B, empty square symbols).

ing the working distance, since the source is mounted on a z manipulator. The natural linewidth of the radiation is lower than 1 eV, which is sufficient for XPS to determine binding energies of core levels within 0.2 eV.

2. EUV source

Two systems in IMPACT rely on the use of EUV sources. One is the EUV photoelectron spectroscopy system and the other is an EUV reflectometry system. The latter is more frequently used than the former. The most important component of the EUV reflectometry and EUPS systems is the light source. Constrains regarding the space limitations and the ease of incorporation into the design were critical in selecting the adequate source. A Roentgen-type source with a silicon anode was used which emits radiation centered at 13.5 nm (92 eV).[20] The source has a steady power output of 10 μW/sr on the 13.5±1 nm; however, the source opening limits the exit solid angle to 0.03 sr, so the net power output of the source is 250–300 nW. This power, assuming a mean energy of 92 eV, corresponds to a photon current of 10^{10} photons/s.

Since the EUV beam is not visible at the sample, the actual size of the EUV beam needs to be determined using an alternate method. The method chosen was to use a masked on EUV reflecting sample and a detector. The detector used was an EUV photodiode with an active area of 1×1 cm^2 deposited with Si/Mo layer which transmits radiation in the wavelength window of 10–16 nm. A quarter of the EUV reflecting surface is uncovered and the rest covered by a nonreflective material, in this case graphite, as shown in Fig. 7. The sample is tilted to an angle expected to give nonzero reflection, between 46° and 48°, and then is slowly retracted from the chamber. The reflected radiation is measured using an EUV photodiode. The distance retracted can be correlated to the location with respect to the center of the reflective region. It is clear from the figure that the maximum reflectivity should occur when the sample is retracted by 6 mm. The results from the measurement are shown in Fig. 8, which has two sets of data: One corresponds to the sample orientation depicted in Fig. 7 (case A) and is plotted with filled symbols. The other set is obtained by rotating the sample 90° counterclockwise and repeating the measurements (case B). This is done in order to determine the beam symmetry with respect to the dotted line that bisects the sample shown in Fig. 7.

From Fig. 8, it can be seen that the maximum reflectivity is obtained between 6 and 8 mm. A Gaussian fit to the data reveals that the peak reflectivity occurs at 6.7 mm retraction for case A and at 7.7 mm for case B. The discrepancy of the results may be due to the angle of incidence of the light into the sample with respect to the motion axis and also due to the elliptical shape of the EUV footprint on the sample. The beam size is calculated by taking one-half of the Gaussian curves in Fig. 8 and taking the derivative since the measurement is integral. The estimated spot size diameter for the EUV light is 3 mm, but this size is not corrected for the elliptical shape of the footprint and the angle of incidence of the light with respect to the motion axis of the sample. However, this measurement is sufficient to determine that the EUV light spot is small enough to be completely included in the areas of the sample that are modified during an experiment in IMPACT, which normally range from 0.25 to 0.50 cm^2 rastered/exposed areas.

D. Electron-beam evaporation source

A four-pocket electron-beam evaporator (EGN-4, Oxford Applied Research) is installed in IMPACT to expose samples to a thermal source of particles. The e-beam evaporator is also used to deposit ultrathin multilayer films. Currently, the evaporator is set to work with Sn and Li; however, up to four materials can be used at one time. The evaporator has also been custom designed to operate facing downward, which is particularly difficult for low-melting metals such as Sn and Li. The evaporator is calibrated *in situ* with a quartz crystal microbalance (QCM) that lies on a manipulator whose axis lies perpendicular to the axis of the evaporator. Calibration of the evaporation flux is conducted before each experimental series. The deposition rate of a particular vapor species can be measured for different power levels on the evaporator. The evaporator has current monitors near the exit of the crucible, which measure ion current between the ground and the crucible or rod containing the evaporated material. This ion current is proportional to the evaporative flux by a constant factor, which is material dependent. The electron-beam evaporator is equipped with an *in situ* current monitor for closed-loop operation regulating the particle cur-

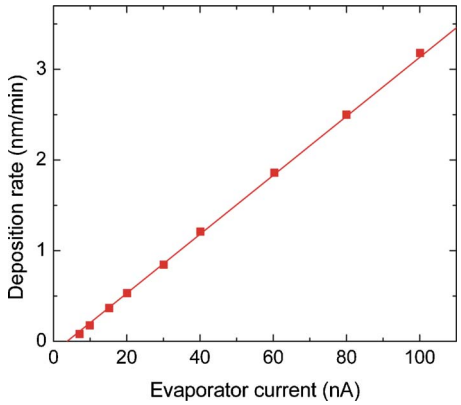

FIG. 9. (Color online) Calibration of e-beam evaporator using a quartz crystal microbalance. The deposition rate measured by the quartz crystal microbalance is calculated using Eq. (1).

rent from the evaporator. This is accomplished by sampling a small fraction of the vapor, which is intrinsically in an ionized state. Once the current is set, the mass gain of the crystal is monitored until a constant slope in the crystal frequency is established. This step is repeated for different current values and a plot of the QCM frequency slope versus evaporator current is generated. The deposition rate measured from the QCM can be calculated from the Sauerbrey equation:[21]

$$\frac{dx}{dt} = \frac{N_{\mathrm{AT}}\rho_{\mathrm{QCM}}}{f_0^2\rho_{\mathrm{evap}}}\left(\frac{df}{dt}\right). \tag{1}$$

Here, x is the deposited thickness in nanometers, dx/dt is the deposition rate in nm/s, N_{At} is the frequency constant of AT cut quartz (in the present case, it is 166 100 Hz cm), ρ_{QCM} is the density of the QCM crystal (2.649 $\mathrm{g/cm^3}$), ρ_{evap} is the density of the deposited film, f_0 is the natural oscillation frequency of the QCM crystal, and df/dt is the slope of the QCM frequency response. This formula assumes that all evaporated flux is collected by the quartz crystal oscillator (QCO) and that the sticking probability is unity at the surface of the QCO. The *in situ* calibration was found to be necessary due to variation in slope of the deposition rate versus evaporator current plot. This variation is, namely, due to the cone used to collimate the vapor beam to a spot within the 1 $\mathrm{cm^2}$ sample area. Over 90% of the vapor is lost to the inner wall of the collimator limiting the deposition rate. Figure 9 shows *in situ* calibration of evaporator using a QCO showing the variation of deposition rate with respect to evaporator current.

E. Hemispherical electrostatic analyzer

IMPACT uses a hemispherical energy analyzer (HSA),[22] which performs energy separation on charged particles emitted from the sample, either electrons (AES, XPS, EUPS), scattered ions (LEISS), or charged recoils (DRS). Energy dispersion can be conducted for a kinetic energy range between 0 and 3500 eV using a 150 mm diameter electrostatic hemispherical deflector. The analyzer has a drift tube with ten electrostatic lenses and an iris located before the hemispherical capacitor (HC) entrance slit. Both entrance and exit slits, are selectable as well, and after the HC exit slit, a five-channel electron multiplier detector collects the energy-dispersed particles. Multiple lens modes are allowed, each one suited for a different application. Magnification modes reduce the collection area to a small (0.2×0.2 $\mathrm{mm^2}$) region to perform spatially resolved studies, point transmission for small excitation sources (such as focused ion and electron beams), and large collection area for measuring average contents over a large sample area. Energy resolution down to <10 meV is possible with narrow energy dispersion,[23] so the identification of elements and their chemical state is reliable due to the high-energy resolution of the analyzer, as it will be shown later in this paper. For ultrahigh-energy resolution applications (e.g., EUPS), the retardation voltage can be operated in a 400 or 40 V range with extremely low ripple having an energy resolution down to 80–800 μeV with pass energies up to 200 eV.

F. Quartz crystal microbalance dual crystal unit

The quartz crystal microbalance technique is a mature and well-developed diagnostic metrology tool measuring mass loss from materials irradiated by energetic particles.[24–26] Measurement of the partial sputter yield requires elemental analysis on the QCO collecting the multispecies sputtered plume material. Typically, this method requires extraction of the QCO from the vacuum chamber for *ex situ* analysis or postirradiation analysis in the IMPACT experiment. This process is time consuming and exposes the QCO sample to atmosphere. The QCM-DCU is installed on a predesigned port of the IMPACT vacuum chamber to address this issue. In QCM-DCU, one crystal oscillator measured the deposition from an eroding surface, while the second measures the background ambient simultaneously. This also contends with the variability of the oscillators with long-temporal, temperature-dependent effects. The ultrasensitive oscillator can pick up background ambient changes and thus when measuring ML level deposition over a relatively small dose, the use of a deposition and reference oscillator system can improve measurement accuracy. Further details of this diagnostic system can be found in the literature.[27,28]

A special port was designed to allow *in situ* surface analysis of the QCO. The port lies at an angle of 145° with respect to the chamber longitudinal axis and when spun 180°, the QCO is rotated to the main sample (after retracting the sample) location exposing the QCO to all surface analysis techniques discussed in the next section. The QCM-DCU system is also translated along its rotational axis and can be removed into a separate load-lock chamber for replacement of QCM crystals or mounting of witness plates. The QCM-DCU is equipped with an *in situ* heater coupled to a detector for temperature control of the oscillator. Temperature-frequency, *T-f*, behavior is calibrated prior to experiments to operate at a temperature where the *T-f* reaches a minimum or maximum.

There are additional advantages with the rotating QCM-DCU setup in IMPACT. One advantage is the ability to measure the collected fraction at multiple points in the space surrounding the sample. This measurement can ultimately lead to an estimate of the sputtered angular distribution of eroded species. The position of the center of the QCM-DCU system is specified by a vector in cylindrical coordinates

(R,z,θ), where R is the fixed radial position of the QCM-DCU on the cylinder, 9 mm. The location along the rotational axis of the QCM-DCU (z) is set to 0 at the point where a normal from the center of the QCO intersects the center of the sample. The value of $\theta=0°$ is set when the center of the sample and the center of the QCO lie on the same vertical plane. The analysis is simplified, given the pair (z,θ), expressing the following integral in terms of those two parameters: $\int_{\Omega_{QCM}} f(\Omega)d\Omega$. Here, $f(\Omega)$ is an angular function representing the sputtering flux and Ω_{QCM} is the solid angle subtended by the QCM-DCU collection oscillator crystal. The procedure to perform the integral over the area of the QCM is outlined in detail in a different publication.[29]

III. ANALYTICAL DIAGNOSTIC TOOLS

IMPACT uses several *in situ* metrology techniques that are able to measure the local surface atomic concentration of implanted or deposited atoms during either exposure to ions or thermal atoms, respectively. *In situ* techniques include LEISS, AES, XPS, and EUPS. All these techniques can interrogate the sample during exposure at various depths. LEISS gives compositional information about the top monolayer in the sample, while AES and XPS probe the subsurface layers. The surface sensitivity of XPS and AES is a result of short attenuation length of electrons in the material under analysis and these techniques can be used for elemental identification and chemical bonding information. Both XPS and AES are useful for determining the elemental composition of the sample as a function of depth.[30]

A. Low-energy ion scattering and direct recoil spectroscopy

Low-energy ion scattering spectroscopy is one of the few real-space techniques able to probe the first and second monolayers of a surface.[3,19] This is possible due to the high ion-atom cross sections and high neutralization rates for probing noble-gas scattering ions. With the use of an electrostatic energy analyzer, the energy of the scattered ions can be determined, and by use of binary collision theory, the mass of the atom from which the ions scattered can be determined.

IMPACT consists of seven ports on which ion sources can be mounted for LEISS measurements. The ports lie on a plane parallel to the viewing axis of the HSA detector, as shown in Fig. 1. In the forward scattering geometry, the laboratory scatter angles of 20°, 45°, 65° can be used. In the backward scattering geometry, the angles of 110°, 130°, and 150° can be used. Normal incidence (90°) ion scattering is also possible. Two ion sources can be used for simultaneous LEISS, which can be useful in measuring inelastic scattering effects from certain projectile/target combinations.[31] Therefore at any given time, two ion sources are used simultaneously on any of the seven ports available (note that the system must be vented in order to change the port location for both ion sources).

To obtain the best mass resolution, large scattering angles and low mass ratios are desirable. The mass ratio can be modified by choosing the mass of the probing beam; however, inert ions of high Z are more prone to neutralization due to their low ionization potentials. We primarily use two different species of ion beams to conduct LEISS and DRS analyses in IMPACT. He^+ ion beams with energies between 1 and 5 keV and Ne^+ ion beams at 2 keV are used, both produced with an NTI 1401 ion source. The purpose of using two different gases for sources of ions is that the heavier the ion beam is, 20 amu for Ne^+ and 4 amu for He^+, the better mass resolution is attained for larger mass atoms, while a lighter ion beam is capable of detecting lighter elements. For studies on heavy-ion implants in high-Z materials, this is an important factor since masses between Sn and Ru or Mo are close and optimization of mass resolution is important. The downside of using a heavier element, such as Ne, is that it will not scatter off lighter elements (i.e., H, C, N, O), so these lighter elements are only visible in the form of direct recoils (direct recoil spectroscopy) in forward geometry. In addition, neon's relatively higher sputtering yield also makes it difficult to work with compared to helium. To avoid inducing extensive damage and mixing of the surface layers, the ion beam flux is carefully controlled to yield the lowest dose possible over the course of a measurement (integrated over many data sets). Typical data acquisition times range from a few seconds to nearly 120 s. The flux is minimized by lowering both ion beam current to levels from tens to hundreds of nanoamperes and beam sizes to >2 mm. The *in situ* QCM-DCU system is used also to guide in real time when the LEISS ion beam induces sputtering (which can be inherently linked with mixing). Typical doses from the LEISS ion beam range from 10^{14} to 10^{15} cm^{-2}, which is an order of magnitude or more less than the dose required to remove a ML from the surface and lower than the threshold for preferential sputtering and ion beam induced mixing.[32]

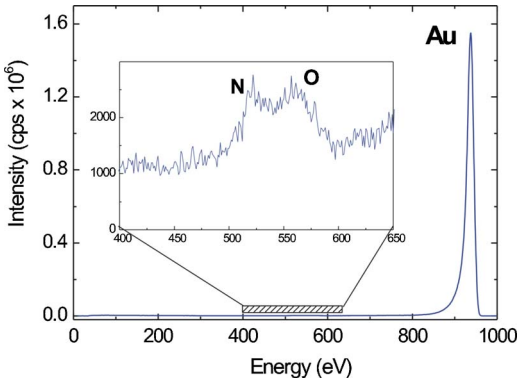

FIG. 10. (Color online) LEISS scan taken with 1 keV He^+ of a bulk Au sample using the normal scattering position (90°). The elemental information is marked in the figure. The inset shows the presence of oxygen and nitrogen impurities on the sample surface.

An example of the sensitivity in LEISS measurements is shown in Fig. 10 for gold. Note that even relatively small amounts of impurities (N and O) are still detected by the HSA. The LEISS spectrum is obtained with 1 keV He^+ bombardment at normal incidence. The scattering angle was set to 90° by installing the ion beam source perpendicular to the detector's line of sight. The intensity from the LEISS spectrum is converted to an atomic concentration for the measured species using the elastic cross section for the He–Au,

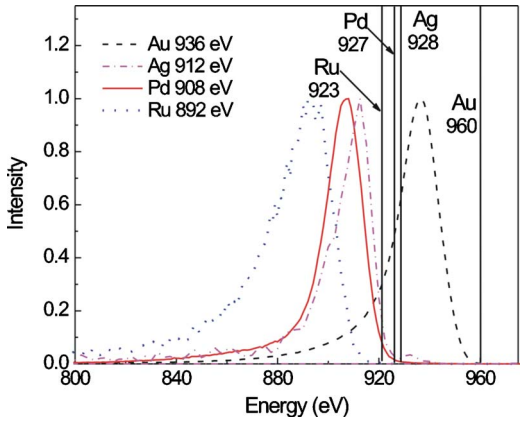

FIG. 11. (Color online) LEISS scans of different elements obtained by measuring the energy of 1 keV He^+ scattered at 90° from the incident direction. The straight solid lines shown in the figure are the expected theoretical locations on the energy spectrum of the corresponding masses measured.

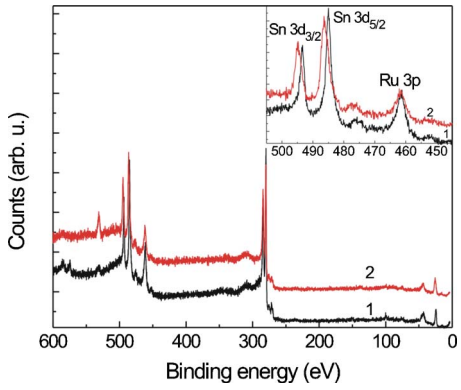

FIG. 12. (Color online) XPS spectra obtained from Sn deposited Ru substrate for two different experimental conditions: (1) *in situ* XPS spectrum of Sn deposited sample with a Sn flux of 5×10^{16} cm^{-2} and (2) XPS spectrum of the above-mentioned sample after air exposure. Inset shows the shifts in Sn 3*d* photoelectron peaks due to oxidation.

He–N, and He–O interactions. The atomic fraction of each component y_i can be calculated by

$$y_i = \frac{A_i\sigma_i^{-1}}{\sum_{k=1}^{N} A_k\sigma_k^{-1}}, \tag{2}$$

where N is the number of peaks each with area A_i, and σ is the elastic scattering cross section. The scattering cross section decreases with increasing target mass and increasing projectile energy. To find the cross-section values, a computer code was written by Bastasz and Eckstein[33] that uses angular differential scattering cross-section equations. The scattering formula used in the code is the Gauss-Mehler quadrature and both screening and potential functions are ZBL. For the example shown in Fig. 10, we convert the relative intensities from the measured spectrum to absolute intensities using Eq. (2). Using the elastic scattering code, we find that the cross sections for 1 keV He^+ scattered at a 90° laboratory angle from Au, N, and O are 32.7×10^{-3}, 3.07×10^{-3}, and 3.70×10^{-3} $Å^2/sr$, respectively. The relative surface concentrations using the corresponding peak areas from Fig. 10 are therefore 0.969, 0.017, and 0.014 for Au, N, and O, respectively.

Determination of concentrations using LEISS can be difficult due to neutralization effects, surface morphology, and impurity surface concentration. However, studies show that matrix effects are minimal using LEISS since the energy of ion scatterers can range from 100 to 5000 eV.[34]

A series of measurements of scattered 1 keV He^+ was performed on pure materials in order to compare the values obtained in practice for the scattered particle energy with values from elastic collision theory. Results of LEISS spectra are shown in Fig. 11. The straight solid lines show the expected theoretical locations on the energy spectrum of the corresponding masses measured. The data result in that the measured energy is always lower than the energy predicted by elastic collision theory. The shifts are always lower than 10% in energy, but even small shifts can mean large uncertainty (~20%) in the mass due to poor mass resolution at the higher energies. The shifts are due to inelastic energy losses during the scattering event, energy spread of the LEISS beam, and in some cases multiple collisions at the surface.

Inelastic energy losses are not uncommon and are handled by design of specific experiments able to measure such losses.[35] Nevertheless, semiquantitative analysis is possible with LEISS since the losses are known when comparing to peaks such as oxygen or other elements known to exist in the sample analyzed. In addition, IMPACT utilizes more than one surface analysis technique to ensure that element identification is properly obtained and verified.

B. Electron spectroscopies

IMPACT applies three types of electron spectroscopies that probe different spatial scales at the surface of ultrathin film systems. The first is x-ray photoelectron spectroscopy using the dual-anode x-ray source described earlier. The second is Auger analysis and the last is extreme UV photoelectron spectroscopy. This section focuses on the first two techniques used in conjunction with other surface characterization tools in IMPACT. Both XPS and AES are useful for determination of atomic surface composition using different procedures of quantitative analysis and they are complementary to each other.[30,36] XPS line shape analysis provides qualitative information and identification of changes in the chemical state of atoms and complex molecules and hence it is a versatile tool for *in situ* surface analysis.

XPS is the energy analysis of the photoelectrons created by x-ray radiation. The ability to perform XPS is valuable when studies regarding the chemical state of elements are of importance, since photoelectron lines shift when elements are in a chemically bound state compared to the pure element. These chemical shifts range from fractions of eV to a few eV. The resolution of chemical shifts is strongly dependent on the energy spread of the measured peak and the magnitude of the shift. An example of XPS *in situ* diagnostics in IMPACT is depicted in Fig. 12 and it shows the photoelectron spectra of Sn deposited on a Ru substrate. The two spectra given in the figure were recorded with identical conditions except for the second spectrum which was taken after exposing the sample to air. It is apparent from the figure that

(see inset of Fig. 12) the Sn 3*d* peaks are shifted toward higher binding energy due to oxidation. A weak oxygen peak (O 1*s*, 532 eV) is evident in the *in situ* XPS spectrum of Sn doped Ru sample and the origin of oxygen may be from the Sn source. The intensity of O 1*s* peak increased considerably after the air exposure. Quantitative analysis of XPS spectra with CasaXPS (Ref. 37) showed that oxygen and tin fractions changed from (0.3, 0.17) to (0.12, 0.33) after air exposure. Ru contributes the remaining atom fraction. These data clearly point out the importance of *in situ* surface analysis.

In surface analysis, it is advantageous to have high spatial resolution of the system. We examined the spatial resolution obtainable with IMPACT XPS system. Two basic approaches for obtaining the highest spatial resolution for XPS are manipulating the source and/or detector parameters. The x-ray source in IMPACT is nonmonochromatic and hence not collimated. So the x rays flood the entire sample area ($\sim 1 \times 1$ cm^2) and photoelectrons are emitted from all places in the sample. The optical elements on the energy analyzer can be used for narrowing the field of view of the detector. The base resolution of a spectrometer is given by the following equation:[38]

$$I \propto \frac{\pi}{4}\left(\frac{r}{M}\right)^2 \alpha\beta, \tag{3}$$

where I, r, and M are the transmitted intensity, the diameter of the input aperture, and the magnification of the transfer lens, respectively, and α and β correspond to acceptance angles in the dispersion and nondispersion directions. The above relation shows, in the absence of spherical aberration, that the spatial resolution is r/M. The transfer lens system in the detector is capable of providing a maximum magnification of 10 and the entrance slit diameter widths can be varied from 1 mm upward. Hence the best spatial resolution obtainable with our XPS is ~ 100 μm by discarding all aberrations caused by the lens system. However, there exists a trade-off between the electron flux and slit value. With the narrowest slit configuration (1 mm), the electron flux reaching the detector is found to be very low. So we opted a configuration of $M=10$ and $r=3$ mm for our measurements which leads to a theoretical spatial resolution of 300 μm by discarding aberrational effects.

To test this capability, a reference sample containing a strip of Teflon with 1.3 mm width is selected. The sample holder in the IMPACT system can provide a translation movement with a resolution better than 10 μm. F 1*s* XPS line scans were taken across the target with 150 μm spatial intervals and with a 50 eV pass energy. Figure 13 gives F 1*s* XPS line scan across the sample surface. The F 1*s* line scan shows a flat F 1*s* intensity region for a spatial distance of 0.5 mm and its intensity drops drastically at both sides. A Gaussian fit shows that the full width at half maximum is 0.95 mm and half width at half maximum corresponds to 0.475 mm. From this we concluded that the spatial resolution of the XPS system is better than 0.5 mm.

IMPACT is also equipped with AES for surface analysis. The excitation source for AES is an electron gun. AES is the energy analysis of the Auger electron generated by the electron beam. Similar to XPS, AES is typically utilized for elemental identification, line scan, and other quantitative information. XPS has the ability to analyze the nonconducting materials such as plastics and ceramics with minimum charging effects and has the ability to investigate differences in the chemical state and bonding in the elements, while AES is superior in terms of higher spatial resolution because of the smaller e-beam size at the target. The beam diameter of the e-beam at the target surface is <0.1 mm and, hence, the spatial resolution of AES diagnostic in IMPACT corresponds to the beam size of the e-beam.

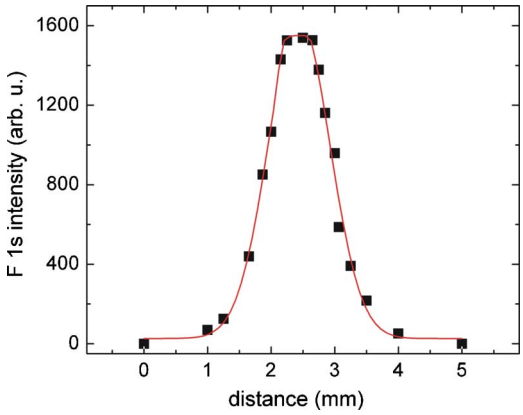

FIG. 13. (Color online) XPS line scan across 1.3 mm wide Teflon sample. F 1*s* photoelectron peak at 689 eV is used.

C. *In situ* erosion rate measurement

IMPACT has a QCM-DCU diagnostic system for *in situ* real-time total erosion measurements to allow for a direct conversion from time to spatial scales during depth profiling with our *in situ* surface analysis metrology. The QCM-DCU diagnostic system measures the deposition of particles on the QCM surface released from the target by sputtering induced by energetic projectiles. It can also provide the absolute sputtering yield induced by energetic charged particles provided the following parameters are known: (a) ion current density, (b) incident particle reflection from the target sputtered *and* from the QCO, (c) the sticking coefficient of sputtered species on the QCO, (d) the fraction of sputtered flux collected by the QCO, and (e) the sputtered azimuthal angular distribution of particles collected by the QCO. These terms and measurements are well documented by Allain *et al.* previously.[39] Quartz crystal microbalances have been used in various configurations to measure small changes in mass during erosion induced by particle bombardment.[40] IMPACT utilizes the QCM diagnostic in collection geometry of sputtered particles as opposed to direct sputter rate measurement by bombarding a predeposited film on the quartz crystal oscillator surface. For multicomponent samples, only the combined mass erosion yield is measured by the QCM-DCU. Details of the QCM-DCU technique are described in Sec. II F. The angular distribution of sputtered particles can be inferred from a set of experimental measurements at different values of z and θ; this technique is to be discussed in detail in a future publication.[41]

Another advantage of the QCM-DCU system is the ability to measure the erosion rate from mixed materials and

redeposited materials. This can be done in several ways. One is to have a polycrystalline thin film deposited on the QCO prior to UHV chamber insertion or deposition *in situ* by exposing the QCO to a sputter target located at the IMPACT sample holder location. Once the film is deposited, a second sputter target can be inserted and bombarded by any of the ion sources available in IMPACT, thus yielding a layered material surface that can be tested as a model surface closely approximating, for example, those of plasma-facing surfaces of thermonuclear fusion devices. Any potential mixing of both target materials can be measured *in situ* after rotating and placing the collector substrate in front of all surface characterization tools in IMPACT. A mixed-material surface can be prepared using any of the ion sources available. In addition once mixing is achieved, ion-induced surface modification can be measured from this mixed-material surface and tracked by several techniques *in situ* and in real time: (1) direct absolute sputter yield measurement from mass loss off the QCO, (2) detection of chemical species with mass spectrometry during irradiation,[42] (3) surface analysis using either LEISS, XPS, EUPS, or AES, and (4) EUV reflectometry for structure determination. Another method for studying redeposited surfaces is to attach a witness plate (typically a specific material desired for study) on the QCM-DCU holder in place of the QCO. This technique only allows the use of surface analysis measurements and is considered useful for only limited cases.

D. *In situ* EUV reflectometry

One of the unique capabilities of the IMPACT facility is the ability to monitor the EUV reflectivity of thin metal films as they are modified, either by an ion beam, a thermal flux, or a combination of both. This capability on IMPACT has already provided important insights relevant to the operation of collector mirrors used in Sn plasma EUV light sources for nanolithography.[11,13]

The EUV source installed in the IMPACT facility emits radiation at 13.5 ± 1 nm. The cone of light leaving the source needs to be collected and transported to the sample. To accomplish that, an elliptical mirror is used. Since we are dealing with EUV radiation that is easily absorbed by most materials, only reflective components can be used. An elliptical mirror with radius of curvature of 0.5 m is chosen to focus the EUV light to a few millimeter spot on the IMPACT target surface location and the half-angle used is 15° with respect to the mirror surface. The collector mirror was manufactured by carving the rough elliptical shape on an aluminum block. The block was electroplated with nickel and then diamond turned to give it the final elliptical shape with an accuracy of 0.002 mm. A reflective 50 nm Ru coating was applied to the Ni mirror at the Optics Fabrication and Metrology laboratory at Argonne's Advanced Photon Source facility. The mirror is mounted on a linear manipulator to allow for small focusing corrections.

The geometry of the reflectometer is sketched in Fig. 14. Two detectors are used in the reflectometer: one for monitoring the reflected light and the other for monitoring the through light. When the sample is retracted, the light can be collected by the through EUV photodiode detector, which

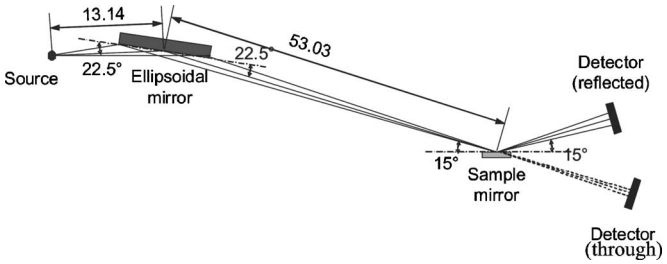

FIG. 14. Schematic of the reflectometer setup in IMPACT. Dashed lines indicate the path of the light when the sample is retracted. Distances are shown in cm.

can be used to monitor the photon flux coming from the source directly. The detectors used in the reflectometer are photodiodes with a 1×1 cm^2 active area and a deposited Si/Mo filter with a spectral band of 10–16 nm photons. This filter greatly reduces the signal due to stray light, but a dark chamber is still required to perform the measurement. Three ports lie on the same plane, which have mounted the EUV beam source, through EUV photodiode, and reflected photodiode. The target coincides with this plane when tilted by 45°. This tilt allows the sample to be probed with any of the surface analysis techniques while the EUV reflectivity is being measured. The half-angle for the reflectivity measurement, as mentioned earlier, is 15° with respect to the plane of the sample.

If all components of the reflectometer were aligned, the peak photocurrent should occur at a tilt of 45°. Small misalignments could exist on the reflectometer setup. Despite these small misalignments, the relative reflectivity measurements can still be performed as long as the conditions of the reflectometer (source position, sample tilt, power output, photodiode efficiency) remain the same during the course of the experiment.

To obtain the relative at-wavelength (13.5 nm) EUV reflectivity as the sample is modified (e.g., temperature, Sn exposure), we consider a sample property that changes with time as $f(t)$ when the sample undergoes a certain treatment. Before the treatment, the value of the photocurrent at the reflectivity detector is recorded as I_0. Both the quantity f and the photocurrent I are measured at a time interval Δt. Then, the reflectivity change due to the change in the property f is obtained by applying the chain rule:

$$\frac{dI}{df} = \frac{dI}{dt}\frac{dt}{df} = \frac{dI}{dt}\left(\frac{df}{dt}\right)^{-1}. \tag{4}$$

By assuming that nothing in the reflectometer changes over the course of the experiment, the relative reflectivity R at any time t is simply given by

$$R(t) = \frac{I(t)}{I_0}. \tag{5}$$

Similarly, the change in reflectivity due to changes in the property f is given by

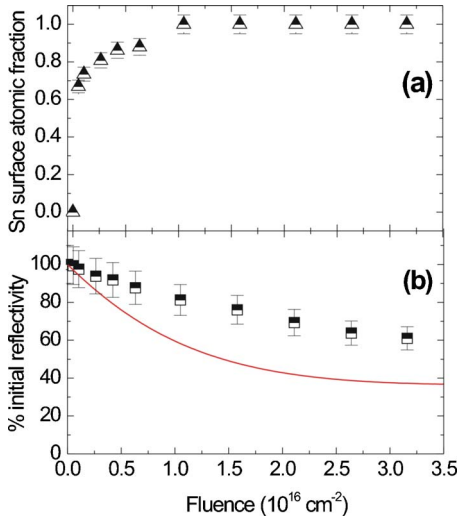

FIG. 15. (Color online) The Sn surface atomic fraction on Rh sample using LEISS for various thermal Sn fluences is given in (a). The Sn fraction reaches a steady state value of 90%–100% coverage at a Sn fluence of about 10^{16} cm^{-2}. The effect on the relative 13.5 nm reflectivity during deposition is given in (b). The solid curve in (b) corresponds to the IMD theoretical Fresnel reflectivity assuming complete monolayer coverage of Sn.

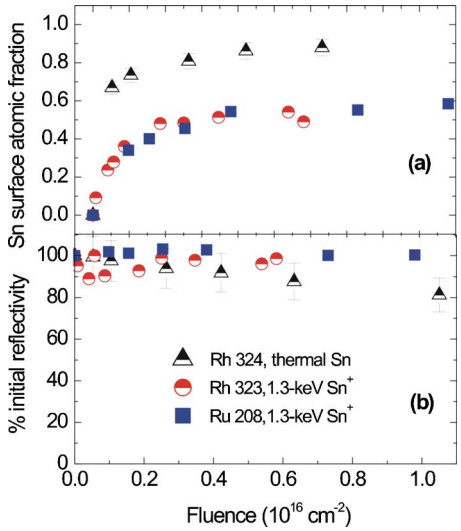

FIG. 16. (Color online) Sn surface atomic fraction measured with LEISS and the relative 13.5 nm EUV reflectivity loss measured with the EUVR are given for energetic and thermal Sn deposition on Ru and Rh substrates.

$$\frac{dR}{df} = \frac{1}{I_0}\frac{dI}{df}. \tag{6}$$

During the course of the experiment, the mechanical components of the reflectometer do not move since all the components are secured to their position, with the exception of the sample under study. The sample is repeatedly retracted to measure the reference intensity from the source on the through detector. This means that the only possible variation on the measured reflected intensity could be attributed to fluctuations in the EUV power coming out of the source. The stability of the EUV power output can be checked during the course of the experiment by monitoring the photodiode located in the line-of-sight of the focused EUV light.

IV. RESULTS AND DISCUSSION

A controlled experiment is used as a model for demonstrating the capabilities of complementary surface characterization techniques used in the IMPACT experiment facility. Results are shown for thin transition-metal films (Rh, Ru, and Pd) exposed to thermal and/or energetic metal Sn particles. The surface is actively probed *in situ* using XPS, LEISS in backscattering mode, QCM-DCU, and EUV reflectometry. EUV reflectometry at 13.5 nm is used to measure the effect on reflectivity from exposure to Sn particles. The results focus on the role thermal versus energetic Sn has on the surface atomic concentration at the mirror surface and the 13.5 nm relative EUV reflectivity.

The first case consists of a Rh mirror exposed to a source of thermal Sn from the e-beam evaporator. Data were taken during Sn exposure using both LEISS and XPS. Simultaneously we measure the effect on 13.5 nm EUV reflectivity with the EUVR system. Figure 15(a) shows the Sn surface atomic fraction measured with LEISS. The surface atomic fraction is measured relative to the Rh concentration omitting any contribution from C and O species. The Sn surface atomic fraction reaches a steady state value of 90%–100% coverage at a Sn fluence of about 10^{16} cm^{-2}. Figure 15(b) shows the effect on the relative 13.5 nm reflectivity during deposition. A comparison is made to the theoretical Fresnel reflectivity using IMD simulations [solid line in Fig. 15(b)]. IMD simulation gives the optical properties of single and multilayer thin films and it assumes layer-by-layer growth (van der Merwe-type).[43] That is, a full monolayer is assumed to grow on the Rh substrate and 100% Sn coverage is reached after a fluence of 10^{15} Sn/cm^2. The results show clearly that the measured 13.5 nm reflectivity is distinctly different compared to the theoretical specular reflectivity from an ideal full Sn layer, suggesting that the morphology and structure of the deposited Sn film are inherently different from those of a van der Merwe-type grown layer. In addition, we noticed that for Sn fluences $>10^{17}$ cm^{-2}, the relative reflectivity at 13.5 nm (15° incidence) from deposited thermal Sn atoms approaches the Fresnel reflectivity to levels near 40%. Further details of the implications of these results are published elsewhere.[41]

The next case studied concerns the exposure of Ru and Rh mirror surfaces to energetic Sn particles compared to one case of thermal Sn deposition. For energetic Sn exposures, 1.3 keV Sn$^+$ at normal incidence is used. Both the Sn surface atomic fraction measured with LEISS and the relative 13.5 nm EUV reflectivity loss measured with the EUVR are shown in Fig. 16 and compared to thermal Sn exposure (sample Rh 234). Energetic Sn at 1.3 keV is expected to implant at two to three MLs into the mirror surface based on previous measurements in IMPACT.[41] Due to a balance between implantation and ion-induced sputtering, the Sn surface atomic fraction reaches a steady state surface concentration that is lower in magnitude compared to Sn vapor deposition. The measured fraction is about 50%–60% and is reached after a Sn ion fluence of about $(0.2-0.3)\times 10^{16}$ cm^{-2}.

The relative reflectivity response of 13.5 nm light from implantation of Sn ions on Rh and Ru mirror surfaces is

invariant for the fluence levels shown in Fig. 16(b). However, for fluence levels ranging between 1×10^{16} and 3×10^{16} cm^{-2} and higher, the relative reflectivity decays to levels between 95% and 98% within the uncertainty of the experiment (~5%). As mentioned earlier, relative reflectivity from deposited thermal Sn atoms for large fluences decays to values near 40% or close to the Fresnel reflectivity. This difference is significant and elucidates on the distinct mechanism between thermal and energetic Sn at the ultrashallow region of the mirror surface from candidate mirror materials (e.g., Ru, Rh, or Pd) and its effect on 13.5 nm reflectivity. One example of the versatility of IMPACT diagnostic facilities is given in a recent article.[44] We studied the in-band mirror reflectivities with exposure to thermal and energetic Sn particles while simultaneously exposing low-energy argon ion beam. In an EUVL setup, an ambient gas can be used to mitigate the energetic debris coming from the plume. However, intense EUV light can partially photoionize background gas used for mitigation in the source device.[45,46] This can lead to weakly ionized plasma creating a sheath and accelerating charged gas particles to the mirror surface inducing sputtering. We simulated a similar environment in the IMPACT facility by providing both sources of Sn (thermal and energetic) *and* low-energy Ar ions (simulating photoionized Ar gas in an EUVL device). The study of the synergistic effect between low-energy ions and Sn particle sources on a candidate EUVL mirror could only be studied in such a setup. Sn atom fraction estimates were made using LEISS and XPS and correlated with in-band reflectivity measured *in situ*.[44]

Another attractive feature of the IMPACT experimental facility is its ability to measure *in situ* the energetic particle-induced erosion rate (sputtering). Recall that this is achieved by a QCM-DCU that is installed on a rotating-translational manipulator system. In this section we consider the total absolute sputtering yield measurement of particles eroded by energetic Sn. A more comprehensive analysis of preferential sputtering is beyond the scope of this paper and is highlighted in a separate publication.[11] During exposure of a Rh sample to 1.3 keV Sn^+, the sputtered material is collected by the QCM-DCU and the sputter rate recorded as a function of time (fluence). Figure 17 shows the raw data from the frequency variation as a function of time (fluence). Precleaning is conducted with a rastered 1 keV Ar^+ beam at near-normal incidence (25°) for a fluence of about 10^{15} cm^{-2} below the threshold for ion-induced surface morphology structure formation. The mirror is then exposed to Sn^+ at 1.3 keV rastered at normal incidence in a 0.25 cm^2 area. Using 6.2 and 4.2 g/cm^3 for the densities of the QCO and Sn eroded film, respectively, the erosion rate is calculated to be about 0.66 nm/s using the expression in Eq. (1), presented earlier in the text. One should note that the irradiation with Sn ions is noncontinuous so that LEISS and XPS data can be taken in between exposures. Therefore the total irradiation time is only about 30 min.

In summary, the IMPACT experimental facility has been designed for versatility in measuring the response of heterogeneous surfaces to a combination of particle sources. By combining Sn thermal atoms and energetic Sn, we have demonstrated the capability of IMPACT *in situ* surface diagnosis including XPS, LEISS, QCM-DCU, and EUVR.

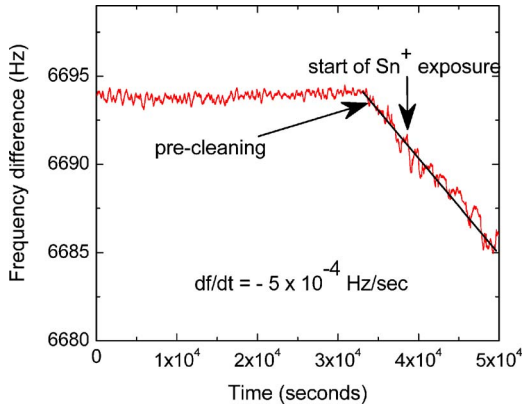

FIG. 17. (Color online) The raw data of QCM-DCU shows the frequency variation as a function of time collected during Rh sample exposure to 1.3 keV Sn ions. Precleaning is done with Ar^+ beam at 1 keV, near-normal incidence with a dose of approximately 10^{15} cm^{-2} below threshold for ion-induced surface structure formation.

ACKNOWLEDGMENTS

We would first like to thank the referees for valuable comments to this manuscript. We would like to especially thank V. Titov and W. Klimowych for work in PRIME facility. We would like to thank our Science Undergraduate Laboratory Internships (SULI) students partly sponsored by the Department of Energy: S. Taj, D. Rokusek, C. Chrobak, E. Hinson, W. Lytle, H. Nomanbhai, M. Hull, and D. Detert. We acknowledge the work of Ph.D. student M. van der Velden of TU Eindhoven for work on threshold sputtering in collaboration with ASML. We would also like to thank our collaborators in EUV lithography work [Philips Research Laboratories in Aachen, Fraunhofer Institut in Aachen, ASML, Xtreme Technologies, NIST-SURF facility, O. Auciello at Argonne National Laboratory (ANL), A. Macrander, and the OFM-APS team at ANL] and work in fusion materials science (R. Majeski and R. Kaita at PPPL, R. Bastasz at SNLL, and R. Doerner at UCSD). We thank A. Egbert of Phoenix EUV for providing EUV source performance data. This manuscript has been created in part by Uchicago Argonne, LLC, Operator of Argonne National Laboratory ("Argonne"). Argonne, a U.S. Department of Energy Office of Science Laboratory, is operated Under Contract No. DE-AC02-06CH11357.

[1] O. Auciello, A. R. Krauss, J. Im, and J. A. Schultz, Annu. Rev. Mater. Sci. **28**, 375 (1998).
[2] W. Jacob, C. Hopf, A. von Keudell, M. Meier, and T. Schwarz-Selinger, Rev. Sci. Instrum. **74**, 5123 (2003).
[3] J. Wayne Rabalais, *Principles and Applications of Ion Scattering Spectrometry: Surface and Chemical and Structural Analysis* (Wiley, New York, 2003).
[4] C. Linsmeier, P. Goldstrass, and K. U. Klages, Phys. Scr., T **T94**, 28 (2001).
[5] M. J. Gordon and K. P. Glapis, Rev. Sci. Instrum. **76**, 083302 (2005).
[6] V. Sizyuk, A. Hassanein, and T. Sizyuk, J. Appl. Phys. **100**, 103106 (2006).
[7] V. Sizyuk, A. Hassanein, and T. Sizyuk, Laser Part. Beams **25**, 143 (2007).
[8] A. Hassanein, J. P. Allain, Z. Insepov, and I. Konkashbaev, Fusion Sci. Technol. **47**, 686 (2005).

[9] S. S. Harilal, B. O'Shay, Y. Tao, and M. S. Tillack, Appl. Phys. B: Lasers Opt. **86**, 547 (2007).
[10] A. Hassanein, T. Burtseva, J. P. Allain, B. J. Rice, V. Bakshi, and V. Safronov, Proc. SPIE **5374**, 122 (2004).
[11] M. Nieto, J. P. Allain, V. Titov, M. R. Hendricks, A. Hassanein, D. Rokusek, C. Chrobak, C. Tarrio, Y. Barad, S. Grantham, T. B. Lucatorto, and B. Rice, J. Appl. Phys. **100**, 053510 (2006).
[12] J. P. Allain, J. N. Brooks, D. A. Alman, and L. E. Gonzalez, J. Nucl. Mater. **337–339**, 94 (2005).
[13] J. P. Allain, A. Hassanein, M. M. C. Allain, B. J. Heuser, M. Nieto, C. Chrobak, D. Rokusek, and B. Rice, Nucl. Instrum. Methods Phys. Res. B **242**, 520 (2006).
[14] J. P. Allain, M. Nieto, and M. R. Hendricks (unpublished).
[15] Nonsequitur Technologies Inc., model: NTI 1401.
[16] Nonsequitur Technologies Inc., model: NTI 1402.
[17] Nonsequitur Technologies Inc., model: NTI 14MS.
[18] J. P. Allain, D. N. Ruzic, D. A. Alman, and M. D. Coventry, Nucl. Instrum. Methods Phys. Res. B **239**, 347 (2005).
[19] H. Niehus, W. Heiland, and E. Taglauer, Surf. Sci. Rep. **17**, 213 (1993).
[20] A. Egbert, B. Mader, B. Tkachenko, A. Ostendorf, C. Fallnich, B. N. Chichkov, T. Missalla, M. C. Schurmann, K. Gabel, G. Schriever, and U. Stamm, J. Microlithogr., Microfabr., Microsyst. **2**, 136 (2003).
[21] B. D. Vogt, E. K. Lin, W. Wu, and C. C. White, J. Phys. Chem. B **108**, 12685 (2004).
[22] SPECS GmbH, model: PHOIBOS 150.
[23] Manual PHOIBOS 150 by SPECS GmbH.
[24] C. H. Skinner, H. Kugel, A. L. Roquemore, J. Hogan, and W. R. Wampler, J. Nucl. Mater. **337**, 129 (2005).
[25] R. Lucklum and P. Hauptmann, Sens. Actuators B **70**, 30 (2000).
[26] R. D. Kolasinski, J. E. Polk, D. Goebel, and L. K. Johnson, J. Vac. Sci. Technol. A **25**, 236 (2007).
[27] J. P. Allain, D. N. Ruzic, and M. R. Hendricks, J. Nucl. Mater. **290**, 180 (2001).
[28] J. P. Allain, A. Hassanein, T. Burtseva, A. Yacout, Z. Insepov, S. Taj, and B. J. Rice, Proc. SPIE **5374**, 112 (2004).
[29] J. P. Allain, M. Nieto, and M. R. Hendricks (unpublished).
[30] P. J. Cumpson and M. P. Seah, Surf. Interface Anal. **25**, 430 (1997).
[31] M. D. Coventry and R. Bastasz, Nucl. Instrum. Methods Phys. Res. B **243**, 193 (2006).
[32] M. W. Sckerl, P. Sigmund, and N. Q. Lam, Nucl. Instrum. Methods Phys. Res. B **120**, 221 (1996).
[33] R. Bastasz and W. Eckstein, *Common Concepts: Particle Scattering Methods of Materials Research* (Wiley, New York, 2000).
[34] W. P. A. Jansen, A. Knoester, A. J. H. Maas, P. Schmit, A. Kytokivi, A. W. Von der Gon, and H. H. Brongersma, Surf. Interface Anal. **36**, 1469 (2004).
[35] M. D. Coventry, J. P. Allain, and D. N. Ruzic, J. Nucl. Mater. **335**, 115 (2004).
[36] W. S. M. Werner, Appl. Surf. Sci. **235**, 2 (2004).
[37] See www.CasaXPS.com
[38] M. P. Seah and G. C. Smith, Surf. Interface Anal. **11**, 69 (1988).
[39] J. P. Allain, M. Neito, M. D. Coventry, R. Stubbers, and D. N. Ruzic, Fusion Eng. Des. **72**, 93 (2004).
[40] G. Hayderer, M. Schmid, P. Varga, H. P. Winter, and F. Aumayr, Rev. Sci. Instrum. **70**, 3696 (1999).
[41] J. P. Allain, M. Nieto, and M. R. Hendricks, "Energetic Sn+ irradiation effects on collector mirror specular reflectivity in the EUV spectral range" (unpublished).
[42] Chemical sputtering is a complex phenomenon and the use of mass spectrometry for its measurement is beyond the scope of this paper.
[43] D. L. Windt, Comput. Phys. **12**, 360 (1998).
[44] J. P. Allain, M. Nieto, M. R. Hendricks, S. S. Harilal, and A. Hassanein, Proc. SPIE **6586**, 6586OW1 (2006).
[45] S. S. Harilal, B. O'Shay, Y. Tao, and M. S. Tillack, J. Appl. Phys. **99**, 083303 (2006).
[46] R. C. Wieggers, W. J. Goedheer, E. Louis, and F. Bijkerk, Proc. SPIE **6586**, 65860L (2007).